CHEMISTRY OF MATERIALS
Cite This: Chem. Mater. 2017, 29, 10139−10149
Article
pubs.acs.org/cm

Quantifying the Fracture Behavior of Brittle and Ductile Thin Films of Semiconducting Polymers

Mohammad A. Alkhadra,[†] Samuel E. Root,[†] Kristan M. Hilby, Daniel Rodriquez, Fumitaka Sugiyama, and Darren J. Lipomi*

Department of NanoEngineering, University of California, San Diego, 9500 Gilman Drive, Mail Code 0448, La Jolla, California 92093-0448, United States

ABSTRACT: One of the primary complications in characterizing the mechanical properties of thin films of semiconducting polymers for flexible electronics is the diverse range of fracture behavior that these materials exhibit. Although the mechanisms of fracture are well understood for brittle polymers, they are underexplored for ductile polymers. Experimentally, fracture can be characterized by observing the propagation of cracks and voids in an elongated film. For brittle polymers, we find that films bifurcate in such a way that the crack density increases linearly with applied strain ($R^2 \geq 0.91$) at small strains. Linear regression is used to estimate the fracture strength and strain at fracture of each material using an existing methodology. For the case of ductile polymers, however, we find that diamond-shaped microvoids, which originate at pinholes and defects within the film, propagate with an aspect ratio that increases linearly with applied strain ($R^2 \geq 0.98$). We define the rate of change of the aspect ratio of a microvoid with respect to applied strain as the "microvoid-propagation number." This dimensionless film parameter, previously unreported, is a useful measure of ductility in thin films supported by an elastomer. To explore the significance of this parameter, we correlate the microvoid-propagation number with nominal ductility using several ductile polymer films of approximately equal thickness. Since the fracture of a film supported by a substrate depends on the elastic mismatch, we study the effect of this mismatch on the propagation of microvoids and observe that the microvoid-propagation number increases with increasing elastic mismatch. Moreover, we find that thicker films exhibit greater resistance to the propagation of fracture. We hypothesize that this behavior may be attributed to a larger volume of the plastic zone and a higher density of entanglements. To understand how the intrinsic mechanical properties of a film influence the fracture behavior on a substrate, we perform tensile tests of notched and unnotched films floated on the surface of water. We find a linear correlation ($R^2 = 0.99$) between the logarithm of the microvoid-propagation number and the fracture stress obtained from tensile tests of unnotched films.

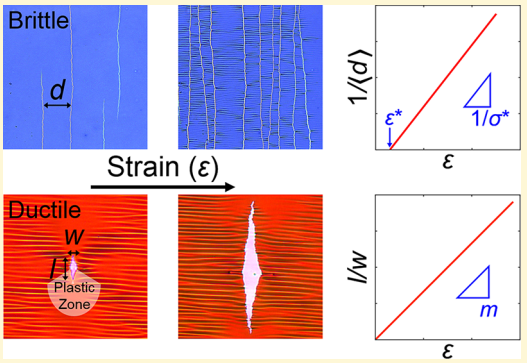

INTRODUCTION

The development of semiconducting polymers that are resistant to fracture requires a comprehensive understanding of their mechanical properties. These materials essentially always take the form of thin films supported by a rigid, flexible, or stretchable substrate. The challenges associated with force-based measurements of the mechanical response of such supported films, however, have led to the development of a suite of optical metrology techniques.[1−4] This paper describes how a range of fracture behavior in films of semiconducting polymers supported by an elastomer can be characterized using optical microscopy (Figure 1). We applied a metrology technique, described by Stafford and co-workers,[2] to thin films of polymers that undergo brittle fracture. In addition, we developed a novel technique to characterize the fracture behavior of thin films of ductile polymers. We quantified the propagation of diamond-shaped microvoids in ductile films using the rate of change in the aspect ratio of these microvoids with applied strain. We then used this methodology to show that the propagation of ductile microvoids is inhibited in thicker films. To supplement these analyses, we performed tensile tests of pseudo-freestanding films—supported only by water—in both notched and unnotched configurations. We then determined quantitative and qualitative relationships between the fracture behavior of a film supported by an elastomer and the mechanical response of the film on water. Our approach should be useful for predicting and comparing the mechanical robustness of thin films of ductile polymers for applications in flexible and stretchable electronics.

THEORETICAL AND EXPERIMENTAL CONSIDERATIONS

The mismatch in elastic modulus (E) between a rigid film and a compliant substrate affects the initiation and propagation of cohesive fracture that channels through the film.[5] For linear elastic films, Beuth showed that the strain-energy release rate

Received: September 18, 2017
Revised: November 18, 2017
Published: November 20, 2017

DOI: 10.1021/acs.chemmater.7b03922
Chem. Mater. 2017, 29, 10139−10149

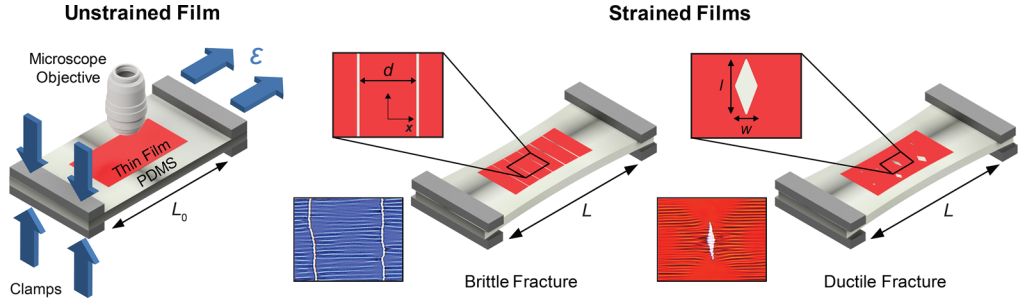

Figure 1. Overview of the experimental methodology and corresponding fracture modes in thin films of semiconducting polymers. Spin-coated film supported by a poly(dimethylsiloxane) (PDMS) substrate is incrementally strained under an optical microscope. Schematic illustrations (top) and representative optical micrographs (bottom) demonstrating fracture by either a brittle or a ductile mechanism. Blue arrows indicate the direction of an applied force, for either clamping or applying tensile strain.

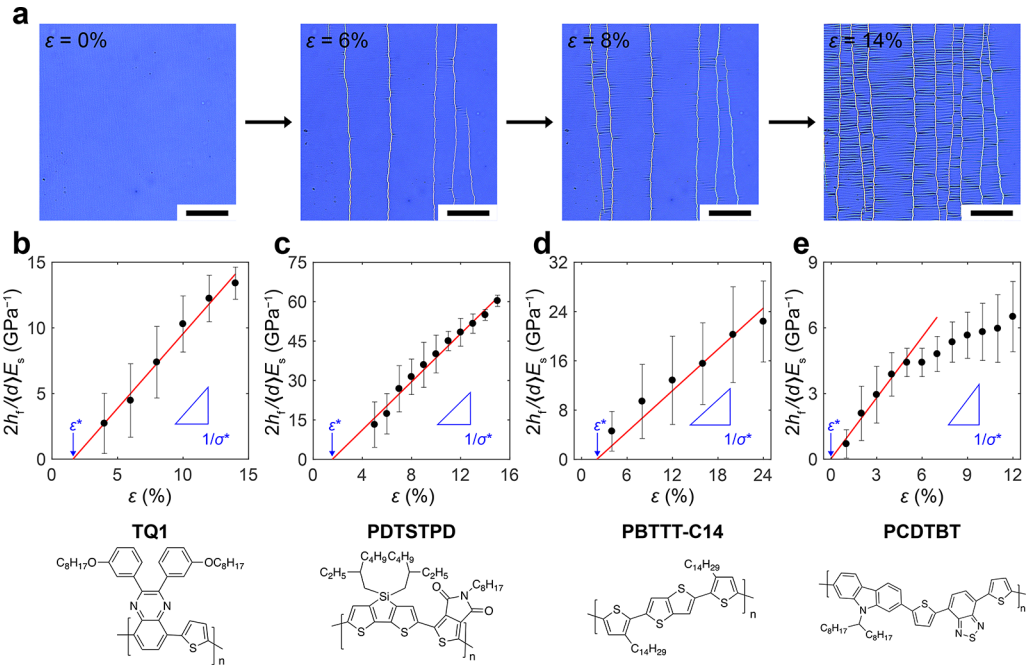

Figure 2. Combined wrinkling−cracking methodology applied to thin films of semiconducting polymers that exhibit brittle fracture. (a) Optical micrographs demonstrating the progressive elongation and systematic fragmentation of a thin film of TQ1 on PDMS; scale bars = 100 μm. Graphs of the scaled crack density $\left(\frac{2h_f}{\langle d\rangle E_s}\right)$ as a function of applied strain (ε) for (b) TQ1 ($h_f = 206 \pm 6$ nm), (c) PDTSTPD ($h_f = 159 \pm 8$ nm), (d) PBTTT-C14 ($h_f = 78 \pm 5$ nm), and (e) PCDTBT ($h_f = 137 \pm 8$ nm). Mean values and error bars (standard deviations) are based on data acquired from at least three separate measurements. Solid red lines correspond to linear regressions. Refer to Experimental Methods for systematic names.

(G, in units of J m^{-2}), defined as the energy dissipated per unit area of fracture surface created, is a function of the elastic mismatch between the film and the substrate.[6] This dependence proceeds from the concentration of stress at the interface of a strained bilayer structure caused by elastic mismatch. Elastic mismatch may be quantified using Dundurs' parameters α and β[6,7]

$$\alpha = \frac{\bar{E}_f - \bar{E}_s}{\bar{E}_f + \bar{E}_s},\ \beta = \frac{1}{2}\frac{\mu_f(1-2\nu_s) - \mu_s(1-2\nu_f)}{\mu_f(1-\nu_s) + \mu_s(1-\nu_f)} \quad (1)$$

where $\bar{E} = E/(1-\nu^2)$, ν is the Poisson ratio, $\mu = E/(2(1+\nu))$, and subscripts "f" and "s" denote the film and substrate, respectively. The dependence of G on β is weak when $\alpha > 0$, in which case β may be neglected.[8] For a stiff film and a relatively compliant substrate, $E_f \gg E_s$ implies that $\alpha \approx 1$. The likelihood for fracture to initiate and propagate increases as Dundurs' parameter α tends to 1 because of the rapid increase in G with increasing elastic mismatch. The Griffith fracture criterion states that fracture occurs when G exceeds the critical value G_c, known as the cohesive fracture energy.[9]

For linear elastic materials, events of fracture may be characterized using the cohesive fracture energy and the stress intensity factor (K), a theoretical construct that relates the applied stress to the intensity of stress near the tip of a crack.[10] For materials that exhibit extensive plastic deformation, however, these parameters of linear elastic fracture mechanics are not sufficient to describe ductile fracture.[11,12] This insufficiency arises because the total energy due to ductile fracture is dissipated not only in the immediate vicinity of the fracture tip but also in an outer region of extensive plastic deformation. To determine parameters for the fracture toughness of ductile materials, the method of the Essential Work of Fracture (EWF) was developed by Cotterell and Reddel.[11] The theory underlying this technique, however,

DOI: 10.1021/acs.chemmater.7b03922
Chem. Mater. 2017, 29, 10139−10149

Table 1. Tabulated Values of the Mechanical Properties Measured Using the Combined Wrinkling−Cracking Methodology. Molecular weights were determined by gel-permeation chromatography (GPC), and glass transition temperatures (T_g) were measured for thin films ($h_f \geq 80$ nm)

material	M_n (kDa) [$Đ$]	h_f (nm)	E_f (MPa)	ε^* (%)	σ^* (MPa)	T_g (°C)
TQ1	4 [1.4]	206 ± 6	120 ± 80	2 ± 2	9 ± 2	∼100, ref 53
PDTSTPD	15 [2.5]	159 ± 8	60 ± 10	2 ± 1	2.2 ± 0.2	110 ± 10, ref 54
PBTTT-C14[a]	6 [2.2]	78 ± 5	180 ± 30	2 ± 2	9 ± 1	102 ± 1, ref 54
PCDTBT	1 [4.3]	137 ± 9	1100 ± 200	0 ± 1	11 ± 3	130 ± 3, ref 29

[a]Spun from a heated solution at $T \approx 80$ °C.

assumes that the sample is not supported by a substrate that can bear the applied load. In the presence of an elastic substrate, adhesion and elastic mismatch strongly influence fracture, while intrinsic mechanical properties such as toughness are less important.[13] In general, the relationship between the intrinsic mechanical properties and the fracture behavior of ductile films supported by a substrate has not been thoroughly investigated.

On the basis of the theory of linear elastic fracture mechanics in thin films,[6,8] a stiffer substrate would delay the onset of fracture and inhibit its propagation, and a more compliant substrate would hasten the onset of fracture and promote its propagation.[5,14] Although the elastic moduli of the polymers we examined spanned multiple orders of magnitude, we standardized the experimental procedure for tensile testing by holding the elastic modulus of the substrate approximately constant at 0.5 ± 0.2 MPa, which is much lower than the moduli of the films. In addition, we studied the role of varying the elastic modulus of the substrate on microvoid propagation in ductile films by varying the ratio of elastomer base to cross-linking agent. We note that this approach also affects the adhesion between the film and the substrate. To simplify our analysis, however, we assume that the film is well bonded to the substrate in all cases.

Fracture may also be influenced by environmental conditions such as moisture, heat, and ultraviolet (UV) radiation.[15] In our experiments, however, effects of heat and UV radiation were trivial due to the controlled environment of the laboratory. We also reduced the influence of moisture content on our samples (e.g., moisture-assisted debonding[15] at the interface between the film and the substrate) by maintaining the relative humidity in our laboratory at approximately 65%.

BRITTLE FRACTURE

Chung and Lee et al. established a methodology that combines wrinkling and cracking of brittle films, such that the elastic modulus, fracture strength, and strain at fracture[16] can be determined simultaneously.[2] This methodology is carried out by transferring a rigid, brittle film onto an elastomeric substrate and incrementally applying uniaxial tensile strain (ε) while measuring the average spacing between cracks (Figure 2a). The validity of this methodology, however, is contingent on the formation of approximately equally spaced, parallel cracks that propagate orthogonal to the direction of applied strain. Such a fragmentation pattern is characteristic of inherently brittle materials whose elastic behavior terminates with rupture—rather than plastic yield—at low strains.[17] In investigating the fracture mechanics of thin films of semiconducting polymers, we observed experimentally that this process of brittle fracture occurs commonly.

The combined wrinkling−cracking methodology is restricted to the case in which the average width of fragments ($\langle d \rangle$) is inversely proportional to the applied strain. It is also assumed that cracks in the film are unaccompanied by yielding or fracture of the substrate, any slip at the film−substrate interface is negligible, and tensile stress (σ) is maximal at the midpoint between adjacent cracks. Under these assumptions, $\langle d \rangle$ is given by[18−20]

$$\langle d \rangle = \frac{2h_f\sigma^*}{E_s(\varepsilon - \varepsilon^*)};\ \varepsilon > \varepsilon^*,\ \langle d \rangle < d_c = \frac{4h_f E_f}{E_s} \tag{2}$$

where h_f, σ^*, and ε^* are the thickness, fracture strength, and strain at fracture of the film, E_f and E_s are the elastic moduli of the film and substrate, respectively, and d_c is the critical width of fragments for which eq 2 is valid.[2] Rearrangement of eq 2 yields a functional form of the scaled crack density $\left(\frac{2h_f}{\langle d \rangle E_s}\right)$ versus applied strain, which allows direct calculation of the fracture strength from the slope of the linear region of the graph. Extrapolation of this linear regression to the x axis $\left(\frac{1}{\langle d \rangle} = 0\right)$ provides a reliable estimate of the strain at fracture. The fracture strength and strain at fracture are closely related to the damage and failure mechanisms of polymer films and, by extension, organic electronic devices.[13]

On applying uniaxial tensile strain, a buckling instability is produced by a transverse compressive strain due to the Poisson effect.[1] A periodic wrinkling pattern with a well-defined wavelength (λ) appears parallel to the direction of applied strain.[2] At low strains and for a sufficiently thick substrate, the buckling wavelength can yield quantitative estimates of the elastic modulus of the film according to

$$\frac{E_f}{1-\nu_f^2} = \frac{3E_s}{1-\nu_s^2}\left(\frac{\lambda}{2\pi h_f}\right)^3 \tag{3}$$

where ν_f and ν_s are the Poisson ratios of the film and substrate, respectively.[1] The elastic modulus of the film is relevant for deformable applications and wearable devices, and it can be tailored to minimize interfacial stress and interlayer delamination that would otherwise result in catastrophic failure of these devices.[13]

We employed the combined wrinkling−cracking methodology to analyze the fracture of films of brittle semiconducting polymers. The mechanical response and fracture of a thin film of TQ1 subjected to uniaxial strain is illustrated in Figure 2a; as shown in Figure 2b, fragmentation occurred linearly with strain. A similar response was observed for thin films of PDTSTPD, PBTTT-C14, and PCDTBT, as shown in Figure 2c, 2d, and 2e, respectively. The large uncertainties associated with the scaled crack densities in Figure 2b and Figure 2d manifest as large errors on estimates of the strain at fracture (refer to Table 1). This uncertainty could be due to the highly statistical nature of crack formation,[21] which depends on film defects and surface

DOI: 10.1021/acs.chemmater.7b03922
Chem. Mater. 2017, 29, 10139−10149

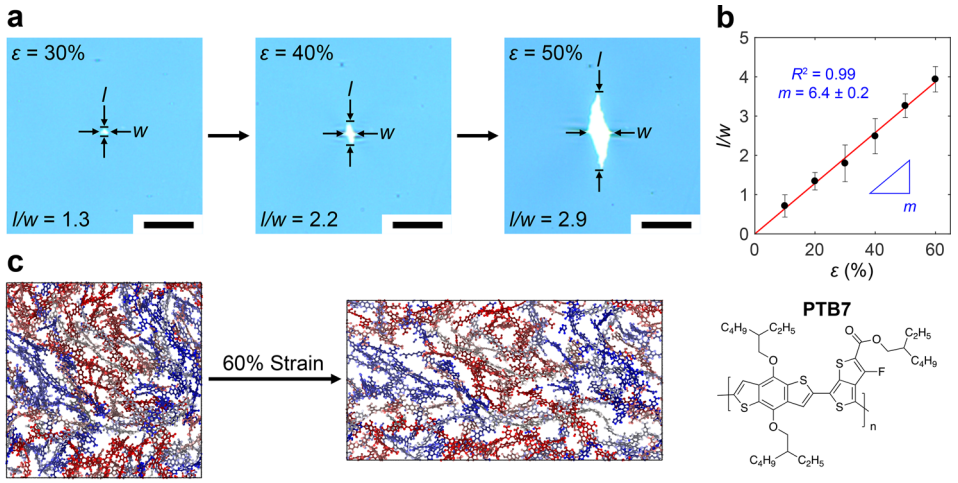

Figure 3. Propagation of ductile microvoids in a thin film of PTB7 (h_f = 110 ± 8 nm and E_f = 90 ± 30 MPa) under tensile strain. (a) Optical micrographs depicting the progressive elongation and consequent growth of a microvoid in a thin film of PTB7 on PDMS; scale bars = 25 μm. (b) Plot of the aspect ratio (l/w) of the microvoid as a function of applied strain (ε). To normalize the relationship for microvoids that appear at different strains, the graph is shifted vertically so that the intercepts pass through the origin. Mean values and error bars (standard deviations) are based on data acquired from three separate measurements. Solid red line corresponds to a linear regression with slope m. (c) A 4 nm slice of a molecular dynamics simulation box showing the molecular yielding of PTB7 with applied strain. Hydrogen atoms are removed for clarity, and separate polymer chains are colored distinctly.

roughness. In contrast, the uncertainties associated with the slopes of the regressions are comparatively smaller, as indicated by the small errors on estimates of the fracture strength.

In Figure 2e, the rate of change of the scaled crack density with respect to applied strain begins to decrease for $\varepsilon \geq 6\%$. Stafford and co-workers attribute such behavior[22] to an insufficiency in the amount of stress induced on the film by the substrate for existing fragments to continue to bifurcate.[2] In any case, the relationship between scaled crack density and strain is linear ($R^2 \geq 0.91$) at low strains, and linear regression was used to determine the fracture strength and strain at fracture. Estimating Poisson ratios of $\nu_f = 0.35$ and $\nu_s = 0.5$,[23] eq 3 was used to calculate the elastic modulus of the film for each material based on the corresponding wavelength of wrinkles produced at low strains. The results of this analysis are summarized in Table 1.

On the basis of the strains at fracture reported in Table 1, the materials examined clearly underwent brittle fracture at low strains. The most plausible explanation for this mechanical response is the relatively low molecular weights of the materials coincident with their relatively high glass transition temperatures (T_g). Semiconducting polymers with molecular weights near or below the entanglement molecular weight comprise unconnected, chain-extended crystals that cannot endure large stresses and, as a result, manifest extreme brittleness.[5,24] In this instance, chain pullout is the favored mechanism of fracture.[25,26] Analogously, semiconducting polymers with T_gs well above room temperature often—though not always—fail in a brittle manner because segmental relaxation cannot occur on short, experimental time scales.[27] Considering the data in Table 1, the materials we examined using the combined wrinkling−cracking methodology fractured near ε = 2%. Moreover, the product of the elastic modulus of the film and the strain at fracture is approximately equal to the fracture strength for each of the respective polymers. These materials therefore absorbed the applied mechanical energy entirely elastically and, in turn, ruptured without exhibiting any plastic yield or deformation, which is characteristic of brittle fracture.[17]

Films of semiconducting polymers exhibit strong, substrate-dependent variations in the T_g with thickness, though these variations occur predominantly when a film is thinned below approximately 80 nm.[28−30] In addition, Chung et al. observed no notable thickness dependence of the mechanical properties of thin films of tantalum and atactic polystyrene over the range of thicknesses investigated in their study (50 nm ≤ h_f ≤ 1000 nm).[2] We thus expect there to be no significant thickness dependence of the mechanical properties of the materials listed in Table 1. Although the combined wrinkling−cracking methodology works well for brittle materials, this type of analysis cannot be applied to ductile materials, which are necessary for applications that demand mechanical compliance and extreme deformability.

DUCTILE FRACTURE

Ductility, in the classical sense, is defined as the capacity of a material to sustain large and permanent deformation under tensile loading.[16] In the field of organic electronics, measuring the crack-onset strain (COS) of thin films of semiconducting polymers on elastomeric substrates has been adopted as the standard method of evaluating ductility.[31] This measure alone, however, does not provide a rigorous standard. One reason is that estimation of the crack-onset strain is limited by the finite resolution of an optical microscope. Another reason is that fracture at defects is by nature highly statistical, and since experimenters are susceptible to confirmation bias,[32,33] visual inspection can be imprecise. The crack-onset strain also provides no information with regard to the propagation of microvoids after their initiation. In fact, consideration of fracture in ductile polymers has been limited to the initiation phase, while the propagation of microvoids has been neglected. A more definitive metric is therefore needed to evaluate the ductility of polymer films supported by an elastic substrate.

For ductile materials, fracture in a film initiates at defects—sites to which mechanical stress is highly localized—and grows progressively with increasing strain.[34] These microvoids, compared to the cracks observed in films of brittle materials,

DOI: 10.1021/acs.chemmater.7b03922
Chem. Mater. 2017, 29, 10139−10149

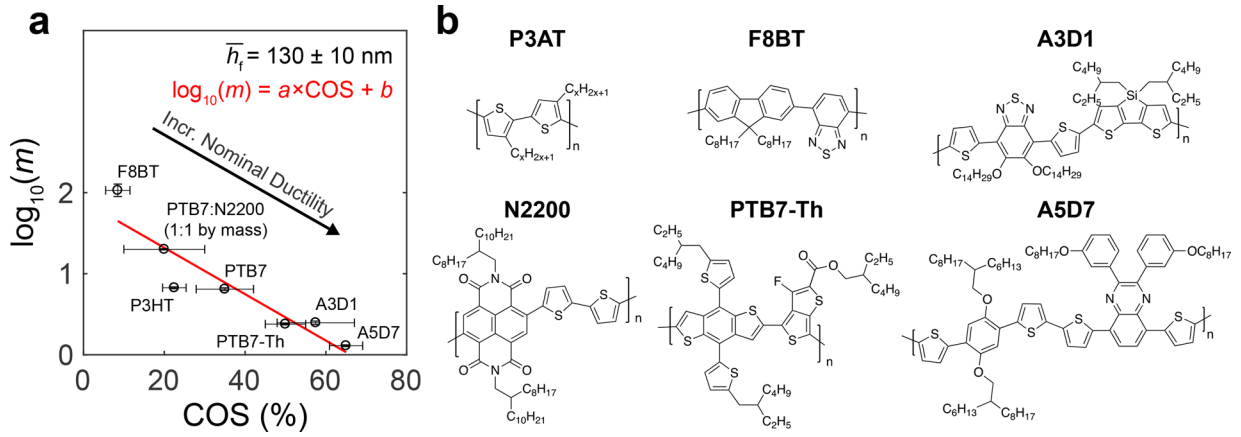

Figure 4. Characterization of ductile fracture using various semiconducting polymers. (a) Correlation of the microvoid-propagation number with nominal ductility for thin films tested at an average thickness of 130 ± 10 nm. Crack-onset strain (COS) is defined as the applied strain at which the length (l) of any existing microvoid in the film (excluding those that are present prior to the application of strain) exceeds approximately 20 μm. Vertical error bars are based on 95% confidence bounds of linear regressions, and horizontal error bars (standard deviations) are based on data acquired from at least three separate measurements. Solid red line corresponds to a linear regression with slope $a = -3 \pm 1$ and y intercept $b = 1.9 \pm 0.6$ (errors are based on 95% confidence bounds). (b) Chemical structures of the materials used to characterize ductile fracture; refer to Experimental Methods for systematic names.

exhibit less of a tendency to propagate with increasing strain, which corresponds to the greater cohesion of ductile materials.[21,35] For the case of PTB7 of high molecular weight, a diamond-shaped microvoid, illustrated in Figure 3a, originated in the film at low strain ($\varepsilon \approx 10\%$) with a small aspect ratio (l/w). Although there existed regions in the film where multiple sites of fracture developed within close proximity to each other, only isolated microvoids were considered for the analysis. As the film was further elongated, we observed that the microvoid propagated progressively with an aspect ratio that increased linearly, as shown in Figure 3b. The rate of change of the aspect ratio of the microvoid with respect to applied strain is given by the slope (m) of a linear regression. This parameter, which we term the microvoid-propagation number, describes the ability of a specimen supported by an elastomer to resist fracture propagation and is an effective measure of ductility.

For events of ductile fracture, elastic strain energy can be dissipated in two ways: through the formation of both cohesive and adhesive fracture surfaces and through the plastic deformation of polymer chains. To portray the molecular mechanism of the process of plastic dissipation, we performed molecular dynamics simulations in which PTB7 was subjected to tensile strain using protocols described elsewhere.[36,37] As demonstrated in Figure 3c, we observed significant morphological rearrangement and alignment of polymer chains. These irreversible deformations ultimately lower the strain-energy release rate that drives the propagation of microvoids. Given that many ductile polymers exhibit such dissipation processes, the formation and propagation of diamond-shaped microvoids is a commonly observed mechanism of fracture in these materials.[35,38] We note that plastic deformation may also take the form of crazing that could occur at the tip of the microvoid. This effect, which commonly occurs in glassy polymers strained below the T_g,[39] would inhibit the propagation of microvoids. Crazing, however, is typically associated with a whitening of the crazed region due to the scattering of light, which was not evident in any of our microscope images.

Nominal Ductility. To correlate the propagation of microvoids with nominal ductility, we measured the microvoid-propagation number and crack-onset strain for a number of semiconducting polymers (Figure 4). We defined the crack-onset strain as the strain at which the length (l) of any existing microvoid in the film exceeded approximately 20 μm. We believe that this is a more rigorous definition of the crack-onset strain that could compensate for limitations in the resolution of optical microscopy and aid in mitigating biases of the experimenter. To further standardize the experimental procedure, films were tested at an average thickness of 130 ± 10 nm. Figure 4a shows a strong correlation between the microvoid-propagation number and the crack-onset strain that can be generalized for thin films of ductile polymers, the chemical structures of which are provided in Figure 4b. Balar and O'Connor determined that crack-onset strain can be correlated with cohesive fracture energy for both brittle and ductile films of semiconducting polymers.[38] Although measuring the cohesive fracture energy is beyond the scope of this work, we expect the microvoid-propagation number to decrease with increasing cohesive energy.

Role of Substrate. Rodriquez and Kim et al. demonstrated that the crack density of thin films of P3HT (40 kDa) supported by PDMS increased with increasing elastic mismatch at a given strain.[5] To examine the effect of elastic mismatch on the propagation of fracture in ductile polymers, we determined the microvoid-propagation number for films of P3BT supported by PDMS of varying elastic modulus, as shown in Figure 5. The results of this experiment indicate that the microvoid-propagation number increases with increasing elastic mismatch and is a stronger function of this mismatch than is the crack-onset strain. This behavior is consistent with the fact that the strain-energy release rate increases rapidly with increasing elastic mismatch. Although adhesive fracture could serve as an additional dissipation mechanism that would inhibit the propagation of microvoids, data obtained from contact angle measurements (refer to Experimental Methods) suggest that the adhesion of P3BT to PDMS of varying elastic modulus (over the range studied) is similar.

In addition to the formation of surfaces of cohesive fracture, adhesive fracture is an important dissipation mechanism that occurs in thin films of polymers supported by a compliant

DOI: 10.1021/acs.chemmater.7b03922
Chem. Mater. 2017, 29, 10139−10149

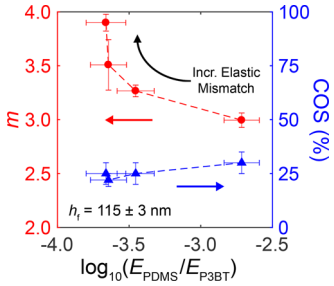

Figure 5. Role of the elastic modulus of the PDMS substrate (E_{PDMS}) on the fracture behavior of films of P3BT ($E_f = E_{P3BT} = 0.25 \pm 0.07$ GPa). Microvoid-propagation number (m) increases with increasing elastic mismatch and is a stronger function of this mismatch than is the crack-onset strain (COS). Dashed lines are guides to the eye.

substrate.[13] Figure 6a illustrates the surface topography of a fractured film of F8BT on PDMS obtained by atomic force microscopy. For ductile polymers, delamination and wrinkling of the film near the center of a microvoid result from the distribution of stress along the length of the microvoid, with the maximum stress being induced at the advancing tip.[17,40] Delamination of a film from the substrate is an important process that dissipates elastic strain energy by diverting it from the propagating tip of a microvoid. This process of interfacial debonding also results in localized necking[41] that could lead to the formation of ductile microvoids.[38] We expect that the adhesion of different semiconducting polymers to PDMS is similar, such that delamination at the center of a microvoid is comparable in all cases.

Role of Film Thickness. In the neighborhood of the tip of a microvoid, there exists a region—the plastic dissipation zone—where energy is dissipated due to plastic deformation.[17] Mai and Cotterell reported that the shape of this plastic zone in bulk samples of ductile engineering and commodity plastics depends on the geometry of the specimen.[12] We therefore investigated the dependence of the propagation of ductile microvoids on the thickness of the film.

The optical micrographs in Figure 6b show the effect of an additional 6% strain on the aspect ratio of microvoids in films of F8BT of different thicknesses. Microvoids in a thicker film, in contrast to a thinner one, propagate with an aspect ratio that is comparatively less sensitive to applied strain, as demonstrated in Figure 6c. The graph of the microvoid-propagation number as a function of the thickness of the film is plotted in Figure 6d, from which the strong dependence on thickness of the rate of propagation of microvoids in ductile films becomes evident. Since the initiation of microvoids is statistical and not all microvoids originate at a specific applied strain, we underscore the significance of the rate of propagation of microvoids—as opposed to the magnitude of the aspect ratio—in its dependence on thickness. In contrast to the microvoid-propagation number, the crack-onset strain exhibited little to no dependence on thickness (Figure 6d); films of F8BT of varying thickness (159 ± 5 nm $\leq h_f \leq 370 \pm 10$ nm) had a crack-onset strain of 9% ± 3% on average. This result strongly indicates that the microvoid-propagation number and the crack-onset strain, although correlated, capture distinct aspects of ductile fracture in thin films of semiconducting polymers. The crack-onset strain is a manifestation of the degree of nonuniformity in a film,[38] and it depends on the relative dimensions of local inhomogeneities and the thickness of the film.[13]

The dependence of the microvoid-propagation number on the thickness of the film may be ascribed to the greater sensitivity of the cohesive fracture energy to thickness in samples of high molecular weight.[42] Compared to polymers of low molecular weight, there is a greater tendency for polymers of high molecular weight to exhibit interchain entanglement, which leads to larger plastic zones around the tips of

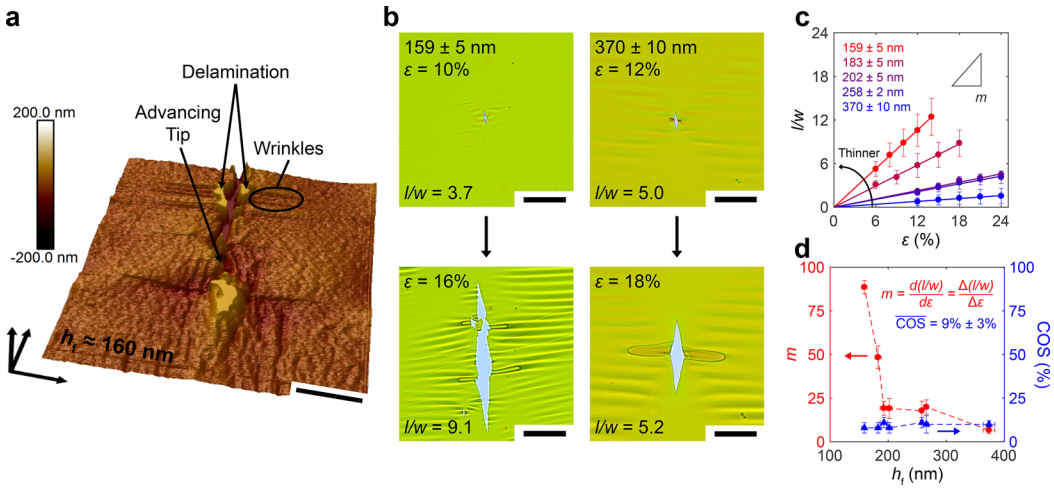

Figure 6. Topography of a cracked surface and dependence of ductile fracture on thickness in films of F8BT ($E_f = 1.0 \pm 0.3$ GPa). (a) Atomic force micrograph (tapping mode) of the height image of a crack in a strained film of F8BT supported by PDMS; scale bar = 3 μm. (b) Optical micrographs depicting the effect of an additional 6% strain (ε) on the aspect ratio (l/w) of microvoids in films of F8BT of different thicknesses; scale bars = 50 μm. (c) Graphs of the aspect ratio as a function of applied strain for films of different thicknesses. To normalize the relationship for microvoids that appear at different strains for a given thickness, the graph is shifted vertically so that the intercepts pass through the origin. Mean values and error bars (standard deviations) are based on data acquired from at least three separate measurements. Solid lines correspond to linear regressions. (d) Graphs of the microvoid-propagation number (m) and the crack-onset strain (COS) as functions of thickness (h_f). Vertical error bars on m are based on 95% confidence bounds of regressions in c; vertical error bars on COS (standard deviations) are based on data acquired from at least three separate measurements; mean thicknesses and horizontal error bars (standard deviations) are based on data acquired from at least five separate measurements. Dashed lines are guides to the eye.

DOI: 10.1021/acs.chemmater.7b03922
Chem. Mater. 2017, 29, 10139−10149

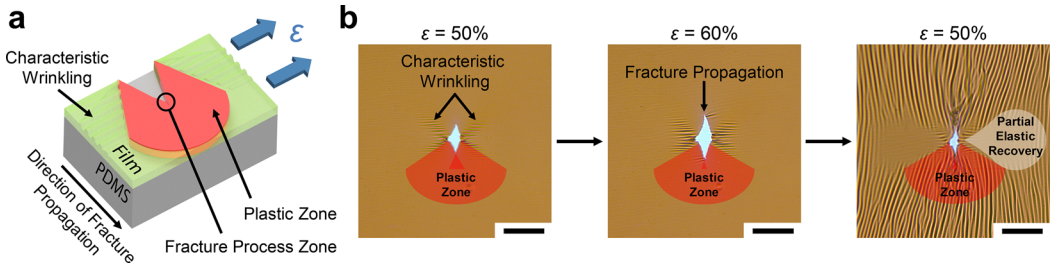

Figure 7. Approximate geometry of the plastic zone in thin films of ductile semiconducting polymers that form diamond-shaped microvoids upon fracture. (a) Schematic illustrating a strained film on PDMS and the proposed shape of the plastic zone under conditions of plane stress. Blue arrows indicate the direction of applied tensile strain (ε). (b) Optical micrographs depicting the effect of an additional 10% strain, followed by the release of this applied strain, on the topography of a film of P3BT (h_f = 115 ± 3 nm); scale bars = 50 μm. Zone ahead of the advancing tip of the microvoid exhibited severe wrinkling upon release of the additional strain; regions horizontally adjacent to the microvoid displayed no such wrinkling.

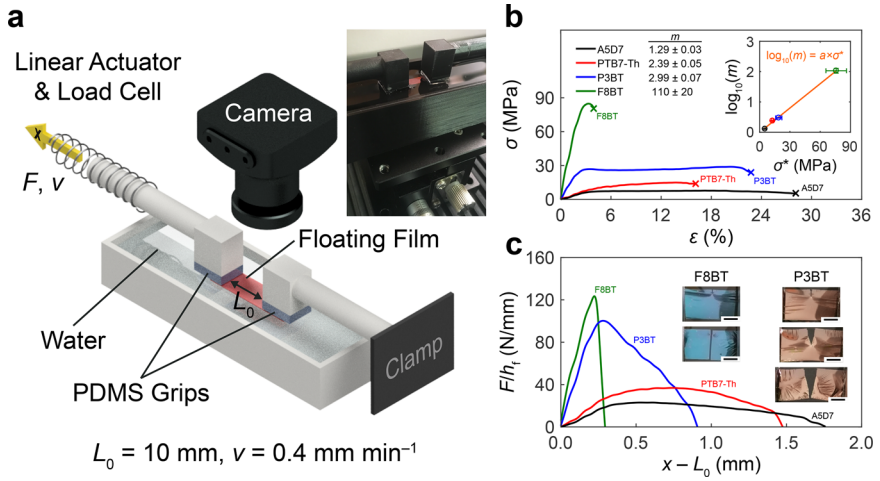

Figure 8. Tensile testing of pseudo-freestanding films of semiconducting polymers. (a) Schematic diagram of the experimental setup, which consists of a linear actuator, a load cell, and a camera. (b) Representative stress–strain curves of unnotched films obtained using the film-on-water technique. (Inset) Plot of the logarithm of the microvoid-propagation number ($\log_{10}(m)$) versus fracture strength (σ^*); values of m are for films tested at an average thickness of 130 ± 10 nm. Horizontal error bars (standard deviations) are based on data acquired from three separate measurements. Solid orange line corresponds to a linear regression with slope a = 0.027 ± 0.001 MPa^{-1} (error is based on 95% confidence bounds). (c) Representative traces of force per unit thickness (F/h_f) versus displacement ($x - L_0$) for notched films of the materials used in b. Notches at the edges of samples were 0.3 ± 0.1 times the width of the respective film, which was equal to 4.5 ± 0.5 mm on average. Inset photographs demonstrate notched samples before and after application of uniaxial strain; scale bars = 2.5 mm.

microvoids.[43,44] Bruner and Dauskardt contended that larger plastic zones inhibit the propagation of fracture by relaxing the stress applied to a film, whereas smaller plastic zones allow extensive propagation of fracture by contributing little to the relaxation of stress.[42] Moreover, Mai and Cotterell argue that the width of the fracture process zone—a necked region of damage that lies directly in the path of an advancing microvoid (Figure 7a)—increases with increasing thickness in thin plates of metals.[12,45] We therefore propose that the plastic zone in a thinner film is geometrically confined by the boundaries of the specimen to a smaller volume, which results in a higher propensity for microvoids to propagate. It is also possible that effects of thin-film confinement—particularly a reduction in the density of entanglements—would lower the cohesion of the film and lead to more rapid propagation of microvoids. From the perspective of theoretical solid mechanics, the problem of relating the propagation of ductile microvoids to the intrinsic mechanical properties of a thin film is currently unsolved. Nonetheless, it would be interesting and useful to learn if a continuum-based approach could be used to predict this dependence on thickness.

Plastic Dissipation Zone. Over the course of this study we repeatedly observed the formation of wrinkles with a characteristic X-shape that appeared around diamond-shaped microvoids, as shown in Figure 6b (right) for instance. We hypothesize that this pattern is determined by the dimensions of the plastic dissipation zone. Figure 7a schematically illustrates a strained film of semiconducting polymer on PDMS under conditions of plane stress (load forces act only parallel to the plane of the thin film). To test our hypothesis and characterize plastic deformation around the tip of a microvoid, we performed a simple experiment in which we partially released the strain applied to an elongated film and inspected the wrinkles that formed in plastically deformed regions.[3] Optical micrographs of a fractured film of P3BT are presented in Figure 7b, the first of which shows these characteristic wrinkles. Elongation of the sample resulted in the propagation of the microvoid, and subsequent release of this additional strain led to severe wrinkling in the zone ahead of the advancing tip. The regions horizontally adjacent to the microvoid, however, displayed no such wrinkling, which suggests the existence of zones of partial elastic recovery.

DOI: 10.1021/acs.chemmater.7b03922
Chem. Mater. 2017, 29, 10139−10149

Tensile Testing of Pseudo-Freestanding Films. It is well known that deformation and fracture in thin films supported by polymeric substrates are influenced by the adhesion and elastic mismatch between the film and the substrate.[46] To isolate these effects from the intrinsic mechanical properties of the film, we implemented a tensile test, originally developed by Kim and co-workers, in which pseudo-freestanding films are supported by water (Figure 8a).[47] The "film-on-water" technique resembles a conventional pull test in that it is used to obtain a trace of force versus displacement in a single step. As shown in Figure 8b, we measured force−displacement curves of unnotched films of four semiconducting polymers and transformed them into stress−strain curves using the dimensions of the corresponding sample. On the basis of these data and the results in Figure 4, we infer that films with a smaller microvoid-propagation number exhibit greater ductility, with or without the support of a substrate. Plotting the logarithm of the microvoid-propagation number versus fracture strength also reveals a correlation between these two parameters, as portrayed in the inset of Figure 8b. The microvoid-propagation number is thus informative of the stress that a thin film under tension can sustain at fracture.

For bulk samples of ductile polymers, the fracture toughness is generally characterized by subjecting a notched specimen to tensile loading while measuring the force.[10,12] To relate the microvoid-propagation number to this classical metric of elastoplastic fracture mechanics, we adapted the film-on-water technique by introducing a notch at the edge of the floating film. This experiment produced curves of force per unit thickness versus displacement, as plotted in Figure 8c. Comparison of these data with the microvoid-propagation number revealed excellent qualitative agreement in the observed behavior. Of the four materials tested, the polymer with the largest microvoid-propagation number, F8BT, exhibited the least ductility: the film bifurcated once the applied load reached a critical value. Conversely, the material with the smallest microvoid-propagation number, A5D7, exhibited significant post-yielding behavior due to blunting at the crack tip. In comparing P3BT and PTB7-Th, the relationship between the propagation of fracture for the cases of films supported by PDMS and by water is more subtle. This subtlety is likely due to the large difference in elastic modulus between these two materials, which introduces effects of elastic mismatch when these films are supported by a substrate. To summarize, tensile testing of films on water revealed that the microvoid-propagation number is related to traditional metrics of the fracture toughness of a freestanding film. Developing an exact, quantitative relationship between the intrinsic mechanical properties—determined for a film on water—and the fracture behavior of the film supported by a substrate, however, demands a thorough theoretical treatment supplemented by further experimental testing and is thus the subject of ongoing research.

CONCLUSION

Understanding the fracture phenomena that govern the mechanical properties of thin films of semiconducting polymers is critical for the design and processing of flexible and stretchable organic electronics. Mechanical failure in polymer films, however, is naturally convoluted and often the consequence of concurrent events of fracture that occur at the molecular scale. Using the combined wrinkling−cracking methodology we quantified the stiffness, strength, and ductility of thin films that exhibited brittle fracture at their respective molecular weights. For films that exhibited ductile fracture, on the other hand, we monitored the growth of isolated microvoids and observed how the aspect ratio varied with applied strain. This measure of the tendency for fracture to propagate was quantified by the microvoid-propagation number, m, which provides insight into the degree of plasticity that a ductile film exhibits. We correlated this previously unreported film parameter with the crack-onset strain for various polymers tested at a common thickness. In addition, we demonstrated that the microvoid-propagation number is a strong function of the thickness of the film, a dependence that may be attributed to the geometry of the plastic zone and effects of thin-film confinement. To better understand how plasticity influences the mechanics of ductile fracture, the molecular-scale phenomena that control the growth of microvoids warrant further investigation. Nevertheless, the microvoid-propagation number should be a useful metric because it serves as a simple yet effective way to evaluate the ductility of thin films supported by an elastomer. The characterization of the resistance of a material to fracture is the backbone of fracture mechanics, and it is crucial in assessing the damage tolerance of semiconducting polymers for mechanically robust electronics.

EXPERIMENTAL METHODS

Materials. Poly(9,9-dioctylfluorene-*alt*-benzothiadiazole) (F8BT, M_w = 20−100 kDa) and poly[*N*-9′-heptadecanyl-2,7-carbazole-*alt*-5,5-(4′,7′-di-2-thienyl-2′,1′,3′-benzothiadiazole)] (PCDTBT, M_w = 20−100 kDa) were purchased from Lumtec and used as received. Poly[2,5-bis(3-tetradecylthiophen-2-yl)-thieno[3,2-*b*]thiophene] (PBTTT-C14, M_n > 12 kDa, $Đ$ = 1.8) was purchased from Solarmer Energy, Inc. and used as received. Poly[(5,6-dihydro-5-octyl-4,6-dioxo-4*H*-thieno[3,4-*c*]pyrrole-1,3-diyl)[4,4-bis(2-ethylhexyl)-4*H*-silolo-[3,2-*b*:4,5-*b*′;]-dithiophene-2,6-diyl]] (PDTSTPD, M_n = 7−35 kDa, $Đ$ = 1.4−2.9), poly[[2,3-bis(3-octyloxyphenyl)-5,8-quinoxalinediyl]-2,5-thiophenediyl] (TQ1, M_n = 12−45 kDa, $Đ$ < 3.3), and poly({4,8-bis[(2-ethylhexyl)oxy]benzo-[1,2-*b*:4,5-b′]dithiophene-2,6-diyl}{3-fluoro-2-[(2-ethylhexyl)-carbonyl]thieno[3,4-*b*]thiophenediyl}) (PTB7, M_w = 80−200 kDa, $Đ \leq$ 3.0) were purchased from Sigma-Aldrich Co. and used as received. Poly(3-butylthiophene) (P3BT, M_n = 50−70 kDa, $Đ$ = 2.1−3.0) was purchased from Rieke Metals, Inc. and used as received. Poly{[*N*,*N*′-bis(2-octyldodecyl)naphthalene-1,4,5,8-bis-(dicarboximide)-2,6-diyl]-*alt*-5,5′-(2,2′-bithiophene)} (PNDI(2OD)-2T, Polyera ActivInk N2200, M_n = 48 kDa, $Đ$ = 3.7) was purchased from Polyera Corp. and used as received. Poly[4,8-bis(5-(2-ethylhexyl)thiophen-2-yl)benzo[1,2-*b*;4,5-b′]dithiophene-2,6-diyl-*alt*-(4-(2-ethylhexyl)-3-fluorothieno[3,4-*b*]thiophene-)-2-carboxylate-2−6-diyl)] (PTB7-Th, M_w > 40 kDa, $Đ$ = 1.8−2.0) was purchased from Ossila Ltd. and used as received. Poly(3-hexylthiophene) (P3HT, M_n = 80 kDa, $Đ$ = 1.6) was produced and characterized by the Heeney laboratory using synthetic procedures described elsewhere.[5] A3D1 (M_n = 50 kDa, $Đ$ = 10.8) and A5D7 (M_n = 34 kDa, $Đ$ = 3.4) were selected from a library of low-bandgap polymers used in studies by Bundgaard et al.[48] and subsequently by Roth and Savagatrup et al.[35] PEDOT:PSS (Clevios PH 1000) was purchased from Heraeus and used as received. (Tridecafluoro-1,1,2,2-tetrahydrooctyl)-1-trichlorosilane (FOTS) was purchased from Gelest, Inc. and used as received. Chloroform, acetone, and isopropyl alcohol were purchased from Sigma-Aldrich Co. and used as received. Alconox was purchased from Alconox, Inc. and used as received.

Gel Permeation Chromatography. Since the suppliers reported wide ranges of molecular weight for some polymers used in this study, we independently measured the molecular weight and polydispersity of these materials using gel permeation chromatography (GPC). GPC was performed in chlorobenzene at 55 °C using an Agilent 1260

DOI: 10.1021/acs.chemmater.7b03922
Chem. Mater. 2017, 29, 10139−10149

separation module equipped with a 1260 refractive index detector and a 1260 photodiode array detector. Molecular weights of polymers were calculated relative to linear polystyrene standards. Our measured values of M_n for the brittle polymers are presented in Table 1. For F8BT, we measured M_n = 10 kDa and $Đ$ = 3.2. For PTB7, the chains eluted too rapidly, such that the peak retention time was outside the range of calibration standards, and thus, no reliable data could be obtained.

Preparation of Substrates. Glass slides were prepared as the substrate for polymer films. The glass slides were cut into squares of 2.5 cm × 2.5 cm using a diamond-tipped scribe and then cleaned in sonication baths of powdered Alconox dissolved in deionized water, pure deionized water, acetone, and isopropyl alcohol for cycles of 10 min each. After sonication, the slides were dried using a stream of compressed air. To activate the surface of glass, improve wettability, and remove any residual organic debris, the slides were treated with air plasma (30 W) for 5 min at a base pressure of 200−250 mTorr. Since TQ1 and PCDTBT adhered too strongly to glass treated in this manner, glass slides treated with antiadhesive FOTS were used as substrates. Specifically, slides were treated with plasma, placed in a desiccator with a vial containing a few drops of FOTS, and then left under vacuum for at least 3 h.

Preparation of Films. Solutions of pure polymers and a blend of PTB7 and N2200 (1:1 by mass) were prepared at given concentrations in chloroform and allowed to stir overnight. After mixing, the solutions were filtered with 1 μm glass fiber media syringe filters before spin coating. All films were then spun, either directly on glass or on a PEDOT:PSS/glass substrate, in two steps. (PTB7-Th was spun from a heated solution at $T \approx 80$ °C.) First, F8BT (20 mg mL^{-1} in chloroform) was spun at 750 rpm (375 rpm s^{-1} ramp), 1000 rpm (500 rpm s^{-1} ramp), 1300 rpm (650 rpm s^{-1} ramp), 1500 rpm (750 rpm s^{-1} ramp), 2000 rpm (1000 rpm s^{-1} ramp), and 3500 rpm (1750 rpm s^{-1} ramp), separately, for 2 min, and F8BT (10 mg mL^{-1} in chloroform) was spun at 1000 rpm (500 rpm s^{-1} ramp) for 2 min. TQ1 and PCDTBT (10 mg mL^{-1} in chloroform) were spun onto glass treated with FOTS at 500 rpm (250 rpm s^{-1} ramp) for 2 min. All other solutions had a concentration of 10 mg mL^{-1} in chloroform and were first spun at 1000 rpm (500 rpm s^{-1} ramp) for 2 min. Second, all films were spun at 2000 rpm (1000 rpm s^{-1} ramp) for 30 s. Thicknesses of films were obtained using a Veeco Dektak stylus profilometer; at least five measurements were taken for each film.

Preparation of PDMS Elastomers. For tensile (compression) testing, poly(dimethylsiloxane) (PDMS) was chosen as the substrate for mechanical measurements. To prepare, 20 g (50 g) of Sylgard 184 Silicone elastomer base was mixed with 2 g (5 g) of Sylgard 184 Silicone cross-linking agent and stirred until cloudy. The mixture was then spread into a Petri dish with a diameter of 15 cm and a height of 1.5 cm. PDMS was degassed by placing the Petri dish in a desiccator under vacuum until the bubbles ceased to be visible. The dish was then placed in an oven preheated to 70 °C for 50 min to allow the PDMS to cure. Next, the PDMS, with an approximate thickness of 1 mm (3 mm), was cut into rectangular slabs of 1 cm × 9 cm. The elastic modulus of these elastomers was determined to be 0.5 ± 0.2 MPa, on average, using an Instron pull tester. To test the role of elastic mismatch on the fracture behavior of ductile films, additional PDMS elastomers were prepared: 20 g of Sylgard 184 Silicone elastomer base was mixed with 1, 1.5, or 2 g of Sylgard 184 Silicone cross-linking agent. This batch of PDMS was then allowed to cure in an oven at 70 °C for 40 min, which resulted in elastic moduli of 54 ± 8, 56 ± 5, and 90 ± 10 kPa, respectively. Otherwise, the preparation procedure was the same as described above.

Combined Wrinkling−Cracking Methodology. Slides with polymer films were scored into four, equally sized rectangular sections. Films of PDTSTPD and PBTTT-C14 were transferred to unstrained strips of PDMS by firmly pressing a scored portion of the film onto PDMS and submerging the film−PDMS bilayer in deionized water. While still in water, the slide with the remaining sections of the film was removed, after which the PDMS was dried with compressed air. Films of TQ1 and PCDTBT were not transferred while submerged in water because they had been spun onto glass slides treated with FOTS. Instead, these films were scored into thin segments, placed onto strips of PDMS, and quickly removed with an applied force directly perpendicular to the film−PDMS interface. The film−PDMS bilayers were then uniaxially stretched at one end using a linear translation stage (L_0 = 1.27 cm), and the mechanical response of each film was imaged using a Leica DM2700 optical microscope.

Microvoid Aspect Ratio. Scored films of ductile polymers were transferred to unstrained strips of PDMS by firmly pressing a scored portion of the film onto PDMS and submerging the bilayer in deionized water. While still in water, the slide with the remaining sections of the film was removed, after which the PDMS was dried with compressed air. The film−PDMS bilayer was then uniaxially stretched at one end using a linear translation stage (L_0 = 1.27 cm), and the mechanical response of the film was probed by observing the growth of isolated microvoids under the microscope.

Buckling-Based Metrology for Measuring Elastic Moduli. Elastic moduli of the brittle films examined using the combined wrinkling−cracking methodology, namely, TQ1, PDTSTPD, PBTTT-C14, and PCDTBT, were estimated by applying the buckling-based metrology of Stafford et al. (eq 3) to these films based on the wrinkling behavior under tension.[1,2] On the other hand, measuring the elastic moduli of ductile films, namely, F8BT, PTB7, and P3BT, required compression-induced mechanical buckling to produce visible wrinkling patterns. As such, neat slabs of PDMS were strained to approximately 5% on a linear translation stage and fixed to rectangular glass slides. For each material, films prepared at three different thicknesses (using spin speeds of 500, 1000, and 1500 rpm with ramp rates of 250, 500, and 750 rpm s^{-1}, respectively) were scored and transferred to the prestrained PDMS. The release of this prestrain produced a buckling instability and, in turn, wrinkles in the films. For each film, the wrinkles were imaged under a microscope at several (>7), arbitrary locations. To count the number of wrinkles in an image, we used a function in MATLAB based on the Savitzky-Golay smoothing filter and peak finder, which distinguishes between crests and troughs. To compute the buckling wavelength (λ), the width of an image was divided by the average number of wrinkles. Moreover, the thickness of the film (h_f) was measured (on glass) using a stylus profilometer, and the elastic modulus of PDMS (E_s) was determined using a commercial pull tester. Finally, the elastic modulus of the film (E_f) was calculated using eq 3.

Molecular Dynamics Simulations. All simulations and visualizations were performed using LAMMPS[49] and OVITO,[50] respectively. A detailed description of the atomistic model parametrization from calculations of electronic structure, as well as the computational process for generating the simulation morphology, can be found elsewhere.[36,51] Briefly, 60 independent 12-mers were packed into a simulation box and subjected to NPT dynamics at 800 K using time increments of 2 fs for 5 ns to generate a well-equilibrated melt phase. This melt-phase structure was then subjected to an annealing protocol in which the temperature was ramped from 800 to 300 K in intervals of 20 K and at time increments of 1 ns for runs of both ramping and equilibration. Simulations of mechanical deformation were run by imposing a constant strain rate (1×10^{-6} Å ps^{-1}) in the x dimension and applying stress-free boundary conditions in both transverse dimensions.

Contact Angle Measurements. To qualitatively assess the adhesion between films of P3BT and strips of PDMS, we measured the advancing and receding contact angles of droplets of deionized water (~6 μL) on pristine surfaces of PDMS. Imaging and data analysis were performed with an automated goniometer (Ramé-Hart, model no. 290-U1) using the method of add/remove volume. Advancing (receding) contact angles of droplets of deionized water on pristine surfaces of PDMS ranged from 119.0° ± 0.6° (109° ± 3°) to 125.9° ± 0.7° (117° ± 4°), which correspond to the PDMS substrates with the highest and lowest elastic moduli, respectively.

Atomic Force Microscopy. A solution of F8BT in chloroform, with a concentration of 15 mg mL^{-1}, was spun onto glass treated with FOTS in two steps (1000 rpm for the first) as described above. A PDMS substrate was prepared as explained above, though its surface was subsequently activated by cleaning with ultraviolet−ozone (UV−

DOI: 10.1021/acs.chemmater.7b03922
Chem. Mater. 2017, 29, 10139−10149

O_3) for 2 h, followed by treatment with FOTS in the same manner that the glass slides were. The film of F8BT on glass was scored into thin segments and transferred to the PDMS treated with FOTS. To generate microvoids in the film, the film−PDMS bilayer was uniaxially stretched at one end using a linear translation stage. Once enough microvoids were produced, the substrate was fixed at the corresponding applied strain. A second, pristine PDMS slab (neither cleaned with UV−O_3 nor treated with FOTS) was prepared by curing at 70 °C for 50 min on the smooth surface of a silicon wafer. After that the slab was cut into squares of 1 cm × 1 cm (approximately 1 mm thick) and used to strip the fractured film off the strained, surface-treated PDMS for imaging. Atomic force micrographs of the height image were then obtained using a Veeco scanning probe microscope (SPM) in tapping mode, and the data were analyzed with NanoScope Analysis v1.40 software (Bruker Corp.).

Film-on-Water Tensile Testing. Kim and co-workers developed a tensile test in which pseudo-freestanding films are supported by water.[47] The "film-on-water" technique resembles a conventional pull test in that it is used to obtain a trace of force versus displacement in a single step. This technique leverages the high surface tension and low viscosity of water to support thin films and allow unimpeded sliding of these films on the surface. To float a specimen on water, a sacrificial layer of PEDOT:PSS—onto which semiconducting polymers were spin coated—was used. (PEDOT:PSS was spun onto a glass slide at 1000 rpm (500 rpm s^{-1} ramp) for 3 min, followed by a second step at 2000 rpm (1000 rpm s^{-1} ramp) for 30 s.) The layer of PEDOT:PSS readily dissolved in water upon contact, which allowed the polymer film to delaminate from the substrate. Once the film was afloat, van der Waals adhesion was made between the film and a load cell using grips coated with small slabs of PDMS. To obtain plots of force versus displacement, films were uniaxially strained at a rate of approximately 6.67×10^{-4} s^{-1} (L_0 = 10 mm) until the test was terminated. Additional tests of fracture were performed by introducing notches at the edges of films, which were then subjected to uniaxial strain. Procedures for preparation and transfer of samples were otherwise identical for films that were and were not notched.

AUTHOR INFORMATION

Corresponding Author

*E-mail: dlipomi@eng.ucsd.edu.

ORCID

Darren J. Lipomi: 0000-0002-5808-7765

Author Contributions

†M.A.A. and S.E.R.: These authors contributed equally.

Notes

The authors declare no competing financial interest.

ACKNOWLEDGMENTS

This work was supported by the Air Force Office of Scientific Research (AFOSR) Grant Number FA9550-16-1-0220. Further support was provided by a gift from the B Quest Giving Fund made through Benefunder to D.J.L. and the Achievement Reward for College Scientists (ARCS) Fellowship awarded to S.E.R. Computational resources to support this work were provided by the Extreme Science and Engineering Discovery Environment (XSEDE) Program through the National Science Foundation Grant Number ACI-1053575.[52] The authors would like to acknowledge the laboratories of Profs. Martin Heeney (P3HT) and Frederik Krebs (A3D1 and A5D7) for providing materials for this study. In addition, the authors would like to thank Prof. Vlado A. Lubarda, Dr. Laure V. Kayser, Dr. Suchol Savagatrup, Dr. Charles B. Dhong, and Cody W. Carpenter for insightful discussion.

REFERENCES

(1) Stafford, C. M.; Harrison, C.; Beers, K. L.; Karim, A.; Amis, E. J.; VanLandingham, M. R.; Kim, H. C.; Volksen, W.; Miller, R. D.; Simonyi, E. E. A Buckling-Based Metrology for Measuring the Elastic Moduli of Polymeric Thin Films. *Nat. Mater.* **2004**, *3*, 545−550.

(2) Chung, J. Y.; Lee, J.; Beers, K. L.; Stafford, C. M. Stiffness, Strength, and Ductility of Nanoscale Thin Films and Membranes: A Combined Wrinkling-Cracking Methodology. *Nano Lett.* **2011**, *11*, 3361−3365.

(3) Printz, A. D.; Zaretski, A. V.; Savagatrup, S.; Chiang, A. S.-C.; Lipomi, D. J. Yield Point of Semiconducting Polymer Films on Stretchable Substrates Determined by Onset of Buckling. *ACS Appl. Mater. Interfaces* **2015**, *7*, 23257−23264.

(4) Savagatrup, S.; Makaram, A. S.; Burke, D. J.; Lipomi, D. J. Mechanical Properties of Conjugated Polymers and Polymer-Fullerene Composites as a Function of Molecular Structure. *Adv. Funct. Mater.* **2014**, *24*, 1169−1181.

(5) Rodriquez, D.; Kim, J.-H.; Root, S. E.; Fei, Z.; Boufflet, P.; Heeney, M.; Kim, T.-S.; Lipomi, D. J. Comparison of Methods for Determining the Mechanical Properties of Semiconducting Polymer Films for Stretchable Electronics. *ACS Appl. Mater. Interfaces* **2017**, *9*, 8855−8862.

(6) Beuth, J. L. Cracking of Thin Bonded Films in Residual Tension. *Int. J. Solids Struct.* **1992**, *29*, 1657−1675.

(7) Dundurs, J. Elastic Interaction of Dislocations with Inhomogeneities. In *Mathematical Theory of Dislocations*; Mura, T., Ed.; American Society of Mechanical Engineers: New York, 1969; pp 70−115.

(8) Xia, Z. C.; Hutchinson, J. W. Crack Patterns in Thin Films. *J. Mech. Phys. Solids* **2000**, *48*, 1107−1131.

(9) Griffith, A. A. The Phenomena of Rupture and Flow in Solids. *Philos. Trans. R. Soc., A* **1921**, *221*, 163−198.

(10) Martinez, A. B.; Gamez-Perez, J.; Sanchez-Soto, M.; Velasco, J. I.; Santana, O. O.; Ll Maspoch, M. The Essential Work of Fracture (EWF) Method - Analyzing the Post-Yielding Fracture Mechanics of Polymers. *Eng. Failure Anal.* **2009**, *16*, 2604−2617.

(11) Cotterell, B.; Reddel, J. K. The Essential Work of Plane Stress Ductile Fracture. *Int. J. Fract.* **1977**, *13*, 267−277.

(12) Mai, Y.-W.; Cotterell, B. On the Essential Work of Ductile Fracture in Polymers. *Int. J. Fract.* **1986**, *32*, 105−125.

(13) Root, S. E.; Savagatrup, S.; Printz, A. D.; Rodriquez, D.; Lipomi, D. J. Mechanical Properties of Organic Semiconductors for Stretchable, Highly Flexible, and Mechanically Robust Electronics. *Chem. Rev.* **2017**, *117*, 6467−6499.

(14) Li, T.; Huang, Z.; Suo, Z.; Lacour, S. P.; Wagner, S. Stretchability of Thin Metal Films on Elastomer Substrates. *Appl. Phys. Lett.* **2004**, *85*, 3435−3437.

(15) Rolston, N.; Printz, A. D.; Dupont, S. R.; Voroshazi, E.; Dauskardt, R. H. Effect of Heat, UV Radiation, and Moisture on the Decohesion Kinetics of Inverted Organic Solar Cells. *Sol. Energy Mater. Sol. Cells* **2017**, *170*, 239−245.

(16) *Mechanical Engineers' Handbook*, 3rd ed.; Kutz, M., Ed.; John Wiley & Sons, 2015; Vol. *1* (Materials and Engineering Mechanics).

(17) Ward, I. M.; Sweeney, J. *Mechanical Properties of Solid Polymers*, 3rd ed.; John Wiley & Sons, 2012.

(18) Volynskii, A. L.; Bazhenov, S.; Lebedeva, O. V.; Ozerin, A. N.; Bakeev, N. F. Multiple Cracking of Rigid Platinum Film Covering Polymer Substrate. *J. Appl. Polym. Sci.* **1999**, *72*, 1267−1275.

(19) Bazhenov, S. L.; Volynskii, A. L.; Alexandrov, V. M.; Bakeev, N. F. Two Mechanisms of the Fragmentation of Thin Coatings on Rubber Substrates. *J. Polym. Sci., Part B: Polym. Phys.* **2002**, *40*, 10−18.

(20) Volynskii, A. L.; Panchuk, D. A.; Moiseeva, S. V.; Kechek'yan, A. S.; Dement'ev, A. I.; Yarysheva, L. M.; Bakeev, N. F. New Approach to Evaluation of the Stress Strain Properties of Nanolayers of Solid Materials. *Russ. Chem. Bull.* **2009**, *58*, 865−882.

(21) Awartani, O.; Lemanski, B. I.; Ro, H. W.; Richter, L. J.; De Longchamp, D. M.; O'Connor, B. T. Correlating Stiffness, Ductility, and Morphology of Polymer:Fullerene Films for Solar Cell Applications. *Adv. Energy Mater.* **2013**, *3*, 399−406.

DOI: 10.1021/acs.chemmater.7b03922
Chem. Mater. 2017, 29, 10139−10149

(22) Heinrich, M.; Gruber, P.; Orso, S.; Handge, U. A.; Spolenak, R. Dimensional Control of Brittle Nanoplatelets. A Statistical Analysis of a Thin Film Cracking Approach. *Nano Lett.* **2006**, *6*, 2026−2030.
(23) Tahk, D.; Lee, H. H.; Khang, D.-Y. Elastic Moduli of Organic Electronic Materials by the Buckling Method. *Macromolecules* **2009**, *42*, 7079−7083.
(24) Koch, F. P. V.; Rivnay, J.; Foster, S.; Müller, C.; Downing, J. M.; Buchaca-Domingo, E.; Westacott, P.; Yu, L.; Yuan, M.; Baklar, M.; Fei, Z.; Luscombe, C.; Mclachlan, M. A.; Heeney, M.; Rumbles, G.; Silva, C.; Salleo, A.; Nelson, J.; Smith, P.; Stingelin, N. The Impact of Molecular Weight on Microstructure and Charge Transport in Semicrystalline Polymer Semiconductors−Poly(3-hexylthiophene), a Model Study. *Prog. Polym. Sci.* **2013**, *38*, 1978−1989.
(25) Washiyama, J.; Kramer, E. J.; Hui, C.-Y. Fracture Mechanisms of Polymer Interfaces Reinforced with Block Copolymers: Transition from Chain Pullout to Crazing. *Macromolecules* **1993**, *26*, 2928−2934.
(26) Washiyama, J.; Kramer, E. J.; Creton, C. F.; Hui, C.-Y. Chain Pullout Fracture of Polymer Interfaces. *Macromolecules* **1994**, *27*, 2019−2024.
(27) Müller, C. On the Glass Transition of Polymer Semiconductors and Its Impact on Polymer Solar Cell Stability. *Chem. Mater.* **2015**, *27*, 2740−2754.
(28) Campoy-Quiles, M.; Sims, M.; Etchegoin, P. G.; Bradley, D. D. C. Thickness-Dependent Thermal Transition Temperatures in Thin Conjugated Polymer Films. *Macromolecules* **2006**, *39*, 7673−7680.
(29) Wang, T.; Pearson, A. J.; Dunbar, A. D. F.; Staniec, P. A.; Watters, D. C.; Coles, D.; Yi, H.; Iraqi, A.; Lidzey, D. G.; Jones, R. A. L. Competition between Substrate-Mediated π-π Stacking and Surface-Mediated T_g Depression in Ultrathin Conjugated Polymer Films. *Eur. Phys. J. E: Soft Matter Biol. Phys.* **2012**, *35*, 129.
(30) Liu, D.; Osuna Orozco, R.; Wang, T. Deviations of the Glass Transition Temperature in Amorphous Conjugated Polymer Thin Films. *Phys. Rev. E* **2013**, *88*, 022601.
(31) Kim, J.-H.; Lee, I.; Kim, T.-S.; Rolston, N.; Watson, B. L.; Dauskardt, R. H. Understanding Mechanical Behavior and Reliability of Organic Electronic Materials. *MRS Bull.* **2017**, *42*, 115−123.
(32) Wason, P. C. On the Failure to Eliminate Hypotheses in a Conceptual Task. *Q. J. Exp. Psychol.* **1960**, *12*, 129−140.
(33) Goldstein, E. B. *Cognitive Psychology: Connecting Mind, Research and Everyday Experience*, 3rd ed.; Cengage Learning, 2010.
(34) Seitz, J. T. The Estimation of Mechanical Properties of Polymers from Molecular Structure. *J. Appl. Polym. Sci.* **1993**, *49*, 1331−1351.
(35) Roth, B.; Savagatrup, S.; de los Santos, N. V.; Hagemann, O.; Carlé, J. E.; Helgesen, M.; Livi, F.; Bundgaard, E.; Søndergaard, R. R.; Krebs, F. C.; Lipomi, D. J. Mechanical Properties of a Library of Low-Band-Gap Polymers. *Chem. Mater.* **2016**, *28*, 2363−2373.
(36) Root, S. E.; Jackson, N.; Savagatrup, S.; Arya, G.; Lipomi, D. J. Modelling the Morphology and Thermomechanical Behaviour of Low-Bandgap Conjugated Polymers and Bulk Heterojunction Films. *Energy Environ. Sci.* **2017**, *10*, 558−569.
(37) Root, S. E.; Savagatrup, S.; Pais, C. J.; Arya, G.; Lipomi, D. J. Predicting the Mechanical Properties of Organic Semiconductors Using Coarse-Grained Molecular Dynamics Simulations. *Macromolecules* **2016**, *49*, 2886−2894.
(38) Balar, N.; O'Connor, B. T. Correlating Crack Onset Strain and Cohesive Fracture Energy in Polymer Semiconductor Films. *Macromolecules* **2017**, *50*, 8611.
(39) McLeish, T. C. B.; Plummer, C. J. G.; Donald, A. M. Crazing by Disentanglement: Non-Diffusive Reptation. *Polymer* **1989**, *30*, 1651−1655.
(40) Serier, B.; Bachir Bouiadjra, B.; Belhouari, M. Finite Element Analysis of Bi-Material Interface Notch Crack Behaviour. *Comput. Mater. Sci.* **2003**, *27*, 517−522.
(41) Li, T.; Suo, Z. Ductility of Thin Metal Films on Polymer Substrates Modulated by Interfacial Adhesion. *Int. J. Solids Struct.* **2007**, *44*, 1696−1705.
(42) Bruner, C.; Dauskardt, R. H. Role of Molecular Weight on the Mechanical Device Properties of Organic Polymer Solar Cells. *Macromolecules* **2014**, *47*, 1117−1121.
(43) Kusy, R. P.; Katz, M. J. Effect of Molecular Weight on the Fracture Morphology of Poly(ethytmethacrylate) in Cleavage. *J. Mater. Sci.* **1976**, *11*, 1381−1384.
(44) Lee, S.; Moon, G. D.; Jeong, U. Continuous Production of Uniform Poly(3-hexylthiophene) (P3HT) Nanofibers by Electrospinning and Their Electrical Properties. *J. Mater. Chem.* **2009**, *19*, 743−748.
(45) Pardoen, T.; Marchal, Y.; Delannay, F. Thickness Dependence of Cracking Resistance in Thin Aluminium Plates. *J. Mech. Phys. Solids* **1999**, *47*, 2093−2123.
(46) Lu, N.; Wang, X.; Suo, Z.; Vlassak, J. Metal Films on Polymer Substrates Stretched beyond 50%. *Appl. Phys. Lett.* **2007**, *91*, 221909.
(47) Kim, J.-H.; Nizami, A.; Hwangbo, Y.; Jang, B.; Lee, H.-J.; Woo, C.-S.; Hyun, S.; Kim, T.-S. Tensile Testing of Ultra-Thin Films on Water Surface. *Nat. Commun.* **2013**, *4*, 1−6.
(48) Bundgaard, E.; Livi, F.; Hagemann, O.; Carlé, J. E.; Helgesen, M.; Heckler, I. M.; Zawacka, N. K.; Angmo, D.; Larsen-Olsen, T. T.; Dos Reis Benatto, G. A.; Roth, B.; Madsen, M. V.; Andersson, M. R.; Jørgensen, M.; Søndergaard, R. R.; Krebs, F. C. Matrix Organization and Merit Factor Evaluation as a Method to Address the Challenge of Finding a Polymer Material for Roll Coated Polymer Solar Cells. *Adv. Energy Mater.* **2015**, *5*, 1402186.
(49) Plimpton, S. Fast Parallel Algorithms for Short-Range Molecular Dynamics. *J. Comput. Phys.* **1995**, *117*, 1−19.
(50) Stukowski, A. Visualization and Analysis of Atomistic Simulation Data with OVITO−the Open Visualization Tool. *Modell. Simul. Mater. Sci. Eng.* **2010**, *18*, 015012.
(51) Jackson, N. E.; Kohlstedt, K. L.; Savoie, B. M.; Olvera de la Cruz, M.; Schatz, G. C.; Chen, L. X.; Ratner, M. A. Conformational Order in Aggregates of Conjugated Polymers. *J. Am. Chem. Soc.* **2015**, *137*, 6254−6262.
(52) John, T.; Cockerill, T.; Foster, I.; Gaither, K. XSEDE: Accelerating Scientific Discovery. *Comput. Sci. Eng.* **2014**, *16*, 62−74.
(53) Kroon, R.; Gehlhaar, R.; Steckler, T. T.; Henriksson, P.; Müller, C.; Bergqvist, J.; Hadipour, A.; Heremans, P.; Andersson, M. R. New Quinoxaline and Pyridopyrazine-Based Polymers for Solution-Processable Photovoltaics. *Sol. Energy Mater. Sol. Cells* **2012**, *105*, 280−286.
(54) Root, S. E.; Alkhadra, M. A.; Rodriquez, D.; Printz, A. D.; Lipomi, D. J. Measuring the Glass Transition Temperature of Conjugated Polymer Films with Ultraviolet-Visible Spectroscopy. *Chem. Mater.* **2017**, *29*, 2646−2654.

DOI: 10.1021/acs.chemmater.7b03922
Chem. Mater. 2017, 29, 10139−10149